


Use of the buffer layers as a current flow diverter in 2G HTS coated conductors

J-H Fournier-Lupien^{1,2} , C Lacroix¹, S Hellmann², J Huh³, K Pfeiffer³ and F Sirois^{1,2}

¹ Polytechnique Montréal, Montréal, QC H3C 3A7, Canada

² Karlsruhe Institute of Technology, Eggenstein-Leopoldshafen, D-76344, Germany

³ Superconductor Technologies Inc. (STI), 9101 Wall Street, Suite 1300, Austin, TX 78754, United States of America

E-mail: j-h.fournier@polymtl.ca

Received 13 June 2018, revised 4 September 2018

Accepted for publication 20 September 2018

Published 12 November 2018



Abstract

This paper presents a simple and effective approach to increase the normal zone propagation velocity (NZPV) in (RE)BaCuO thin films grown on a flexible metallic substrate. The concept is an extension of the current-flow-diverter concept already known in the literature. The key idea behind the novel approach is to use a specific geometry of the silver thermal stabilizer that surrounds the superconducting tape. More specifically, a very thin layer of silver stabilizer is deposited on top of the superconductor layer, typically less than 100 nm, while the remaining stabilizer (still silver) is deposited on the substrate side. Normal zone propagation velocities up to 170 cm s^{-1} at 77 K have been measured experimentally for the first time with this novel architecture, corresponding to a stabilizer thickness of 20 nm on top of the superconductor layer. This is at least one order of magnitude faster than the NZPV speeds measured on commercial 2G HTS tapes. Our results clearly demonstrate that a very thin stabilizer on top of the superconductor layer leads to high normal zone propagation velocities. The experimental values are in good agreement with predictions realized by finite element simulations. Furthermore, the propagation of the normal zone during the quench was recorded *in situ* and in real time using a high-speed camera. Due to high Joule losses generated on both edges of the tape sample, a ‘U-shaped’ profile could be observed at the boundaries between the superconducting and the normal zones, which matches very closely the profiles predicted by the simulations. The most direct application of this new HTS tape architecture is in high field magnets, since faster quench propagation allows easier detection and protection, which is likely to accelerate substantially the development of HTS magnets used as high-field MRI/NMR systems, etc.

Keywords: normal zone propagation velocity, high temperature superconductor, current flow diverter

(Some figures may appear in colour only in the online journal)

1. Introduction

Thanks to their high current density, high mechanical strength and high critical magnetic field, second-generation high-temperature superconductor coated conductors (2G HTS CCs) are candidates of choice for the next generation of devices for high field applications (>20 Tesla, [1]) such as particle accelerators, magnetic confinement fusion and nuclear magnetic resonance. Indeed, the maximum achievable

magnetic field with low temperature superconductors (LTSs) is limited to a value of 23.5 Tesla (DC) [2]. On the other hand, standard 2G HTS CCs made of HTS materials like (RE) BaCuO holds the record for the highest magnetic field ever achieved, i.e. 35.4 Tesla (DC) [3], even reaching a magnetic field of 45 Tesla [4] when used as an insert coil into a resistive magnet.

However, protection against destructive hot spots remains one of the major unresolved issues for the

implementation of magnets based on 2G HTS CCs. The normal zone generated by the hot spot being highly resistive, it produces intense heating, resulting in a rapid local temperature rise (the hot spot) and the destruction of the tape if no protection action is rapidly taken, but the difficulty here is that the time frame allotted to detect a quench is short (in the range of 10–100 ms), so ideally, when a quench occurs, it should propagate rapidly in order to be detected quickly.

In this paper, we propose an original HTS tapes architecture that is at the same time effective to speed up the *normal zone propagation velocity* (NZPV), i.e. the velocity at which the normal zone expands when a hot spot occurs, while being relatively simple in terms of industrial implementation. This architecture was named ‘b-CFD architecture’, for reasons explained in section 2. An extensive experimental characterization of the NZPV was undertaken for different variants of the architecture, namely for various layers of the metallic stabilizer thicknesses on top and bottom of commercial HTS tapes. The NZPV measurements have been realized first by an electrical method, and then by an *in situ* high-speed video recordings of a provoked quench in HTS tapes. Finally, we conducted numerical simulations that reproduced very well all experimental results, suggesting that both the model and our understanding of the underlying physics are correct.

2. State of the art in HTS tapes with accelerated normal zone propagation

The idea of increasing the NZPV in HTS tapes has been substantially investigated in the recent years [5–8]. For wires based on LTS materials, such as Nb_3Sn and NbTi , the NZPV is in the range of 100–1000 cm s^{-1} at 4 K [9], which is fast enough to allow rapid quench detection and protective actions that will avoid irreversible damages. However, the NZPV of 2G HTS CCs is much lower, i.e. 0.1–10 cm s^{-1} [10–15] in the temperature range of 40–77 K. This is mainly explained by the much lower thermal diffusivity of HTS tapes versus LTS wires in the vicinity of their critical temperature, which makes quench detection much more difficult to realize. If one succeeds to increase the NZPV of HTS tapes to values comparable to that observed in LTS wires, the protection of HTS magnets would become much easier [2].

The approaches taken by all authors in the works referenced above are based on the principle that inserting a contact resistance R_i (in $\mu\Omega \text{ cm}^2$) between the superconductor and the metallic stabilizer of HTS tapes allows increasing their NZPV by more than one order of magnitude (see figure 1(a) for a schematic of a typical HTS tape architecture). This has been first shown by numerical simulations [8, 16] and then experimentally [5]. The physical explanation of this phenomenon lies in the increase of the current transfer length (CTL) associated with the increase of R_i [7, 8]. However, from a practical point of view, increasing R_i has the drawback of significantly increasing the heat generation at the contacts for current injection, which is highly undesirable because the tape might eventually burn out.

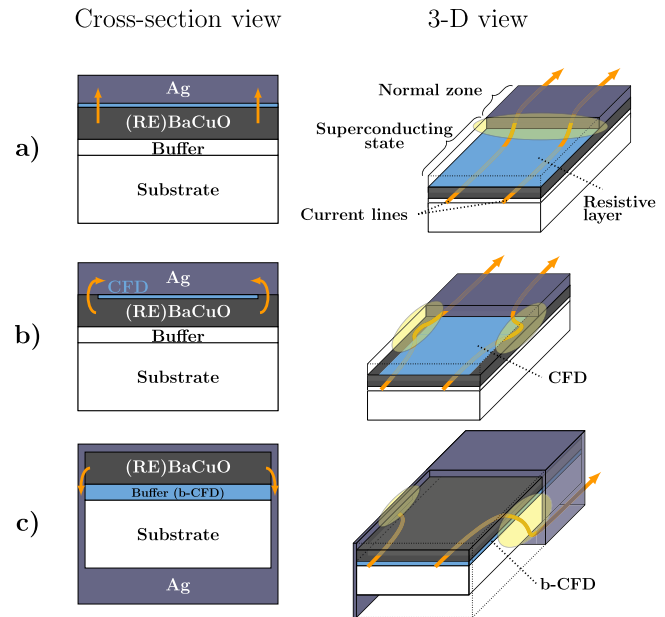


Figure 1. Cross-section views of different tape architectures proposed to increase the NZPV: (a) the uniform architecture, consisting of a uniform interfacial resistance at the Ag/(RE)BaCuO interface (cyan); (b) the ‘classical’ CFD architecture, consisting of a high contact resistance at the Ag/(RE)BaCuO interface (cyan), except at the edges of the tape, where the contact resistance is kept low; (c) the ‘b-CFD’ architecture, in which no high interfacial resistance is needed at the Ag/(RE)BaCuO interface, but which requires a thin top stabilizer and thick bottom stabilizer connected through a conducting edge metallization. The arrows show the current flow paths when the superconductor quenches.

A solution to this problem was proposed in 2014 by Lacroix *et al* [6, 7]. Until then, the contact resistance was uniform across the tape width. We refer to the original architecture as the ‘uniform architecture’ (see figure 1(a)), which is very similar to that of commercially available tapes. The solution introduced in [6] goes one step further by proposing to pattern the contact resistance at the Ag/(RE)BaCuO interface, such as to obtain a very high contact resistance in the middle of the tape and a low contact resistance on its edges. We then obtain the so-called ‘current flow diverter (CFD) architecture’ (see figure 1(b)). In this case, because of the presence of low resistance paths between the stabilizer and the superconductor, it is possible to inject current into the tape without burning the current contacts. This approach is also the first one that explicitly involves a space modulation of the interfacial current density (through the spatial non-uniformity of R_i across the interface), and as a result, for a given value of the global contact resistance, it leads to a much faster NZPV than a purely material-oriented solution.

The explanation behind this major improvement lies in the current concentration occurring in the low contact resistance regions upon current transfer from the superconducting layer to the stabilizer layer, which in turn increases the power density generated at the edges of the tape (yellow regions in figure 1(b)). This partial quench across the tape width speeds up the normal zone propagation substantially, especially for tapes with a thin stabilizer [17], i.e. a few microns at most.

However, for applications such as superconducting magnets, which require a thicker stabilizer (few tens of microns), a solution to increase the NZPV is still sought. Furthermore, from a practical point of view, patterning a contact resistance is *a priori* not straightforward to implement in an industrial fabrication process, involving hundreds of meters of HTS tapes. Therefore, simpler means to implement the CFD concept are also still sought.

In [17], it was proposed that the CFD concept could be implemented without the need to pattern a contact resistance, and in fact, without any additional contact resistance at all at the Ag/(RE)BaCuO interface. This is possible by modifying slightly the stabilizer geometry, as illustrated in figure 1(c). This alternative approach has two major advantages. Firstly, the value of the contact resistance at the Ag/(RE)BaCuO interface can be kept very low. Secondly, the approach remains effective even in the case of a thick stabilizer, which makes it applicable for magnet applications, and any other application requiring a thick stabilizer. Indeed, according to [17], the NZPV can be increased by one order of magnitude in comparison to the case where all the stabilizer is put on the tape, even with a 20 μm thick stabilizer at 10 K.

In the forthcoming sections, we demonstrate experimentally, for the first time, how to increase the NZPV by modifying solely the stabilizer geometry, and nothing else in the classical fabrication process. We call this novel architecture ‘b-CFD’ (for buffer-layer-CFD), since in practice, it is now the buffer layers that play the role of the CFD layer that diverts the current flow through the edges of the tape when a normal zone appears (see again figure 1(c)).

3. Experimental methodology

3.1. Samples preparation

The HTS tape samples used in this work consist of 4 mm wide 2G HTS CCs, custom-made by Superconductor Technologies Inc. in an experimental deposition chamber. The basic template for all samples, depicted in the figure 1(a), consisted of a 0.8 μm thick yttrium–barium–copper–oxygen ($\text{YBa}_2\text{Cu}_3\text{O}_{7-\delta}$) layer grown on a 100 μm thick Hastelloy[®] substrate (C-276TM) by reactive co-evaporation cyclic depositions and reactions (RCE-CDR) deposition method [18]. Lattice matching between the (RE)BaCuO layer and the substrate was realized through a stack of buffer layers composed of $\text{CeO}_2/\text{MgO}/[\text{Y}+\text{Zr}]_2\text{O}_3$ (total thickness of ≈ 0.58 to 0.78 μm).

A 20 nm thick silver (Ag) capping layer has been deposited *in situ* on the (RE)BaCuO layer to ensure a low contact resistance at the Ag/(RE)BaCuO interface. Note that no oxygen annealing treatment has been done on the samples after deposition of the silver layer. Such a treatment, when applied on thin Ag layers (typically less than 500 nm) is known to compromise the integrity of the Ag layer by generating Ag aggregates (islands) when the temperature reaches a few hundred degrees (typically above $\approx 400^\circ\text{C}$ – 500°C) [19].

Table 1. Characteristics of b-CFD samples. Sample S4 is considered as the reference sample.

Sample ID	Top Ag thickness (t_{top} , μm)	Bottom Ag		Total Ag thickness (t_{tot} , μm)
		thickness (t_{bot} , μm)	Ratio ($t_{\text{bot}}/t_{\text{top}}$)	
S1	0.02	≈ 1.98	99	2.0
S2	0.1	1.9	19	2.0
S3	0.3	1.7	5.7	2.0
S4 (ref)	2.0	0.0	0.0	2.0

A total of four samples (4 mm wide by 12 cm long) with different metallic (Ag) stabilizer geometry were subsequently fabricated from the tape template described above. Then, a certain amount of stabilizer (still Ag) was added on the samples using RF sputtering deposition. Our setup allowed sputtering the desired thickness of Ag on the top (superconductor) side (t_{top}) and on the bottom (substrate) side (t_{bot}). We made sure that the total Ag thickness $t_{\text{tot}} = t_{\text{top}} + t_{\text{bot}}$ deposited on each sample was the same, i.e. $t_{\text{tot}} = 2 \mu\text{m}$. The exact Ag thicknesses on each side of the tape are given in the table 1. Special care has been taken to sputter Ag on both edges of the tape in order to electrically connect the top and bottom Ag layers. Furthermore, critical current measurements ($T = 77 \text{ K}$) carried out on each sample revealed that the Ag deposition did not degrade the critical current.

3.2. Measurement of NZPV

The NZPV has been measured using the same setup as described in [5, 6]. A home-made pulsed current source was used to generate square pulses ($\Delta t = 10$ – 20 ms , $I = 55$ – 110 A). A small NdFeB permanent magnet was used to generate a normal zone by lowering locally the critical current I_c . The NZPV was measured using voltage taps in contact with the surface of the tape placed every $\approx 2.5 \text{ mm}$. By measuring the voltage drop generated by the normal zone over time at different locations along the tape, the velocity of the normal zone propagation could be obtained [5]. For all the NZPV measurements, the samples were placed in a liquid nitrogen bath. Note that the NZPV was measured at different locations along the tape and the same value of NZPV was recorded for all location.

3.3. Video recording of the dynamic of the quench

Furthermore, an optical *in situ* study of the quench propagation in liquid nitrogen was also realized, similarly to previous studies reported in the literature [20–23]. The technique consists of quenching locally an HTS tape immersed in liquid nitrogen in order to visualize the propagation of nitrogen gas bubbles. These bubbles, which are generated due to the heat generation at the normal zone location, induce light refraction and multiple reflections at liquid–gas interfaces. This modulates the light intensity received by the detector and create a contrast between the NZ and the superconducting part of the tape. During the experiment, a pulsed current is injected in the

sample and a normal zone is generated by a permanent magnet placed behind the sample. A video is recorded using a MEMRECAM HX high-speed camera (CMOS sensor) from nac Image Technology and an AF Micro-NIKKOR (60 mm $f/2.8D$) lens from Nikon. The high-speed camera is placed behind the double-pane window of a cryostat to separate it from the liquid nitrogen bath. Special care has been taken to prevent bubbles from obstructing the field of view of the camera.

4. Electro-thermal model

A 3D finite element electro-thermal model has been used to simulate the quench behavior of the samples. Details about the model can be found in [7, 17]. The numerical calculations have been realized with the Joule heating module of the COMSOL 4.3b software program, which solves simultaneously the heat equation and the current continuity equation. The coupling of the two equations is ensured through the Joule losses and through the temperature dependence of the electrical parameters.

The geometry of the 3D model consists of a stack of Ag(top)/(RE)BaCuO/Hastelloy/Ag(bottom). We added silver on the sides of the tape to electrically connect the top and bottom Ag layer. Due to symmetrical considerations, we modeled only a quarter of the real tape volume to reduce computational time. The transport current was applied as an integral constraint at one extremity of the tape (i.e. the total current in the superconductor cross-section must be equal to the transport current) and a zero voltage Dirichlet boundary condition ($V = 0$) was applied at the other extremity of the tape, to all layers. The remaining boundaries were electrically isolated, i.e. $\mathbf{n} \cdot \mathbf{J} = 0$, where \mathbf{n} is a vector perpendicular to the boundary. This ensured that the current had no component perpendicular to the remaining boundaries. A heat pulse was applied to one of the extremities in order to generate a normal zone and simulate the effect of the permanent magnet. Finally, the remaining boundaries were considered adiabatic, i.e. $\mathbf{n} \cdot \mathbf{q} = 0$, where \mathbf{q} is the heat flux.

The $E - J$ characteristic of (RE)BaCuO was modeled using an empirical temperature dependent power law $E(J, T) = E_0(J/J_c(T))^{n(T)}$ in the flux creep and flux flow regimes [24], where $E_0 = 1 \mu\text{V cm}^{-1}$ (electric field criterion at 77 K). The transition from the superconducting state to the normal state was modeled as a normal state path in parallel with the superconducting one, such as two resistance in parallel in an electrical circuit. A nonlinear conductivity is derived from the power law model by rewriting it in a form compatible with the constitutive equation $J = \sigma E$, which gives

$$\sigma_{sc}(T) = \frac{J_c(T)}{E_0} \left(\frac{\|\mathbf{E}\|}{E_0} \right)^{\frac{1-n(T)}{n(T)}}, \quad (1)$$

where the temperature dependence of the power law index

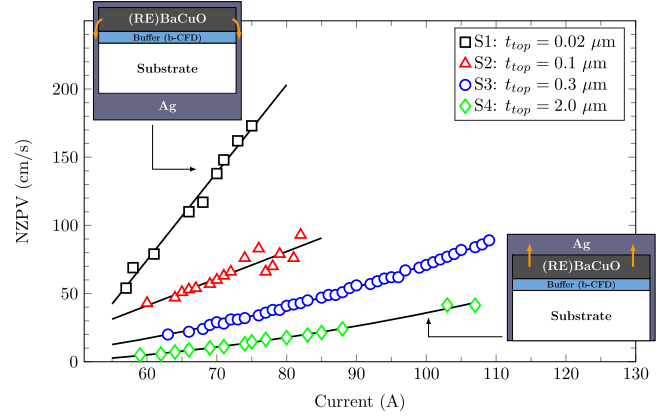


Figure 2. Normal zone propagation velocity as a function of the transport current for different stabilizer thicknesses on the superconductor side. Schematics of the cross-section views of the two extreme cases are shown in the insets. The case with $t_{\text{top}} = 2 \mu\text{m}$ of Ag (green diamonds) is comparable to commercial tapes (no CFD effect) and exhibits the lowest NZPV values. The case with $t_{\text{top}} = 0.02 \mu\text{m}$ of Ag (black squares) shows the highest NZPV values measured. Solid lines are quadratic functions fitted to the experimental data to illustrate the trend.

$n(T)$ has been linearly extrapolated from [25], i.e.

$$n(T) = \begin{cases} (n_0 - 10) \left(\frac{T_c - T}{T_c - T_0} \right) + 10 & \text{for } T < T_c \\ 10 & \text{for } T \geq T_c \end{cases}. \quad (2)$$

The temperature dependence of $J_c(T)$ is considered linear with temperature, i.e.

$$J_c(T) = \begin{cases} J_{c0} \left(\frac{T_c - T}{T_c - T_0} \right) & \text{for } T < T_c \\ 0 & \text{for } T \geq T_c \end{cases}. \quad (3)$$

The parameters J_{c0} and n_0 have been extracted from experimental $I - V$ curves obtained for each sample. The critical current I_c and the exponent n_0 at 77 K of the four samples were in the range of 60–75 A and 18–27 respectively. The tape was 4 mm wide and the (RE)BaCuO layer was $0.7 \mu\text{m}$ thick. This leads to a current density J_{c0} in the range of $1.9\text{--}2.3 \times 10^{10} \text{ A m}^{-2}$ which we used in the model. Simulations were carried out for two values of interfacial resistance between Ag and (RE)BaCuO, i.e. 0.2 and $1 \mu\Omega \text{ cm}^2$. In the simulations, the normal zone has been initiated by applying a local heat pulse at one extremity of the tape. Virtual probes were placed every 1 mm in order to monitor the time evolution of the voltage and the temperature, from which the NZPV can be calculated.

5. Results

5.1. Experiments

The NZPV has been measured experimentally for all samples described in table 1. Figure 2 presents the NZPV values as a function of the transport current for all four samples. First, we

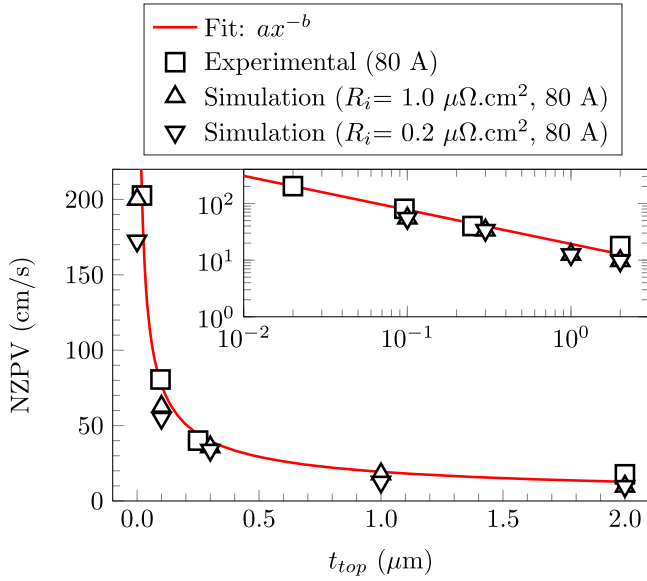


Figure 3. Plot of measured and simulated NZPV values as a function of the top Ag stabilizer thickness (t_{top}), for a fixed transport current of 80 A in all cases. The solid curve shows a fit of the form $y = ax^{-b}$, with $a = 23.0918$ and $b = 0.5333$. Inset: same plot in log-log scale.

observe that the NZPV increases approximately linearly with the current, as expected by the adiabatic model [26]. Indeed, S1 and S2 are well fitted by a linear function, while S3 and S4 are better fitted with a quadratic function, although the curvature is very slight. Furthermore, we observe that, for a given transport current, the NZPV is higher for samples having a thinner layer of Ag on the (RE)BaCuO side (top side) varying from 14 cm s^{-1} when $t_{\text{top}} = 2 \text{ μm}$ (green diamonds) to 171 cm s^{-1} (black squares) when $t_{\text{top}} = 0.02 \text{ μm}$, for $I = 75 \text{ A}$.

Figure 3 present the NZPV values (squares) obtained experimentally for an applied current of 80 A. We observe that the NZPV increases drastically for small values of t_{top} , while it remains almost constant when t_{top} is larger than 1 μm . In the inset, the same results are presented using a logarithmic scale for the x and y axes. The experimental data points can be well fitted with a function of the form $\text{NZPV} = a \cdot (t_{\text{top}})^{-b}$, with $a = 23.0918$ and $b = 0.5333$.

Figure 4 presents snapshots of the nucleation of a normal zone induced by a permanent magnet of 3 mm in diameter placed behind the sample. The generation of the bubbles was recorded in the cases of sample S2 ($t_{\text{top}} = 0.1 \text{ μm}$) and sample S4 ($t_{\text{top}} = 2.0 \text{ μm}$). As observed in figure 4, the normal zone nucleates at the location of the magnet (vertical black line in the middle of the picture) and propagates in the two opposite directions, as indicated by the arrows in the close-up views. When comparing the two snapshots, we observe that the shapes of the normal zones are drastically different. A ‘U-shaped’ profile is clearly visible in the case of sample S2 at both extremities of the normal zone, whereas a quasi-linear profile is observed in the case of sample S4. Those profiles stay roughly stationary while the normal zone is propagating (the propagation stops when the current pulse

ends), then the tape slowly recovers (e.g. the normal zone shrinks until it disappears).

5.2. Comparison with numerical results

In figure 3, we compare the NZPV values obtained experimentally with those obtained by numerical simulations for two values of contact resistance, i.e. $R_i = 0.2$ and 1 μΩ cm^2 . The value of R_i can be adjusted by directly varying the conductivity of the contact resistance at the Ag/YBaCuO interface in the model. The smallest R_i value corresponds to the experimental value measured previously on a commercial tape [5], whereas the highest one was used to quantify the effect of R_i on the NZPV of tapes with the b-CFD architecture. We note that these values are typical for the case of Ag that has been sputtered or evaporated on (RE)BaCuO [19]. We observe that our simulation results are in very good agreement with our experimental results. We also observe that the effect of R_i on the NZPV is much more pronounced in the case of thin layers of Ag on the superconductor side, i.e. small values of t_{top} . Indeed, the numerical value of the NZPV obtained when $t_{\text{top}} = 0 \text{ μm}$ and $R_i = 1 \text{ μΩ cm}^2$ is 200 cm s^{-1} , while for a lower interfacial resistance (0.2 μΩ cm^2), the simulation gives 173 cm s^{-1} . Considering that the NZPV value obtained experimentally in the case where $t_{\text{top}} \approx 20 \text{ nm}$ (sample S1) is 203 cm s^{-1} , it suggests that a value of 1 μΩ cm^2 for the interfacial resistance is more appropriate for the samples considered in the present work.

We note that the difference between the NZPV values obtained with different interfacial resistances quickly becomes negligible as t_{top} increases. When we look more closely at the experimental values versus the values obtained by numerical simulations, we notice that the simulations give in general slightly lower NZPV values. This difference could possibly be explained as follows. Firstly, the non-uniformity of the Ag layers deposited by sputtering, which is known to induce thickness variations in the range of $\pm 50 \text{ nm}$ (according to Dektak thickness profile measurements) is not taken into account in the numerical model. Secondly, the Ag thickness on the edges of the tape is not accurate. In our electro-thermal model, we assumed uniform Ag coating on both faces of the tapes, and a thickness of 1 μm for the Ag on the edges of the tape. The latter number was inferred from the fact that the total thickness of Ag deposited on each sample was 2 μm , but each edge of the sample has been exposed only for one half of the total sputtering time in the chamber (because of the tilted position of the sample in the chamber, used to ensure a good deposition on the edges of the tape). These two factors can likely induce an error in the calculation of the local Joule losses and, therefore, in the calculation of the temperature and NZPV.

The simulated surface temperature distributions of the Ag layer (top view of the 3D model) for each sample are shown in figure 4 below the images taken from the video recording. The parameters used for the simulations are the same as the ones used in figure 3 with $R_i = 0.2 \text{ μΩ cm}^2$. The simulations clearly exhibit the characteristic ‘U-shaped’ profile between the normal zone ($T > T_c$ in red) and the superconducting state

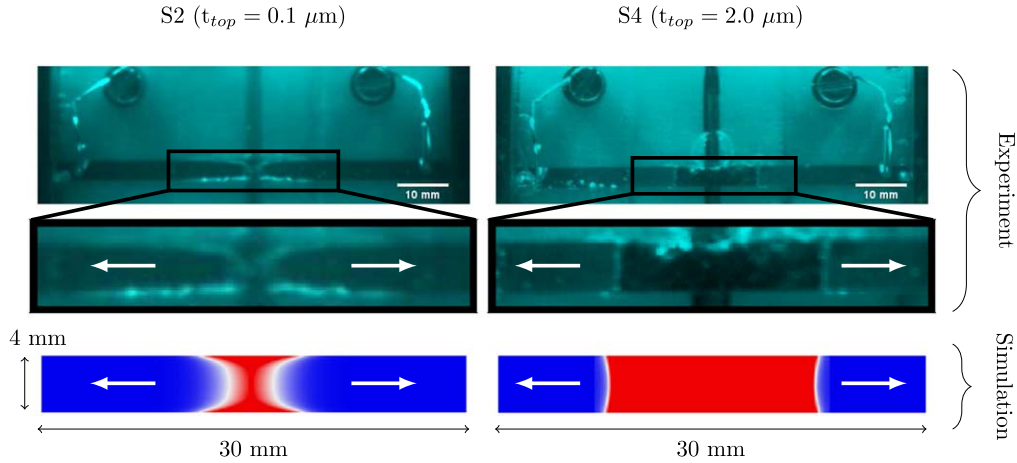


Figure 4. Visualization of the normal zone propagation obtained experimentally (snapshots of a video recorded with a digital high-speed CMOS camera), for two samples: S2 on the left, and S4 on the right. The snapshots show the sample (black horizontal strip) as well as the two voltage taps, at the ends of the sample, held by two screws. The vertical black line in the middle indicate the position of the permanent magnet behind the sample. Below each snapshot, we show a close-up view of the normal zone indicated by the generation of bubbles, which induces a change in the image contrast. The arrows indicate the direction of the normal zone propagation. The current waveform injected in the sample was a square pulse. The snapshot of S2 and S4 have been taken respectively 16 ms after the current had reached 60 A (recorded at 4000 frames s^{-1}), and 40 ms after the current had reached 70 A (recorded at 5000 frames s^{-1}). The distribution of temperature obtained by simulation is shown for comparison under the close-up views for both samples (the simulations were performed with the same parameters as the experimental ones). The normal zone is indicated in red ($T > T_c$) and the superconducting state is in blue ($T = 77$ K). The thin white strips indicate the middle temperature between $T_c = 90$ K and $T = 77$ K, which is about 83.5 K.

($T = 77$ K in blue) observed in the S2 snapshot. The creation of a U-shaped profile is easy to explain considering that, when a normal zone nucleates, the current flowing into the superconductor transfers into the stabilizer by the edges of the tape, as shown in figure 1(c), which generates a very high instantaneous power density (see [17] for more details). The amount of heat that is generated in the edges of the tape during the quench forces the normal zone to initially nucleate in the edges of the tape. Also, we note that the simulations reproduce well the straight superconductor/normal boundary profile observed in the S4 snapshot.

6. Discussion

In a previous study, Levin *et al* [27] were able to find the form of the voltage distribution into the stabilizer in the case of an HTS tape surrounded by a stabilizer, similar to the b-CFD architecture presented in this paper. Their results showed that Joule losses are produced at the edges of the tape when the current transfers from the superconductor layer to the bottom stabilizer layer, similarly to our findings.

Furthermore, as Levin *et al* discussed in their paper, in the case of a large normal zone, the current flowing in the stabilizer fills equally both stabilizer layers (top and bottom) if the thickness of each side is the same, which is quite obvious from basic circuit theory. This means that we can model the two stabilizer layers as two resistances in parallel. Thus, in the case of the b-CFD architecture, since the bottom stabilizer layer is much thicker than the top stabilizer layer, most of the current flows in the bottom stabilizer layer.

Figure 5 presents the current sharing between the different layers along the length of the tape (in the current

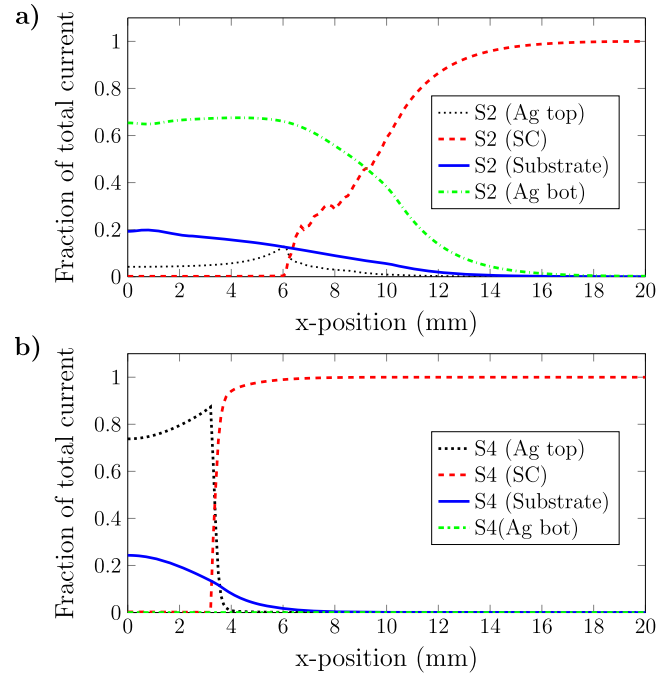


Figure 5. Total current flowing in the different layers of the HTS tape architecture, plotted along the tape length, for samples (a) S2 and (b) S4. Results were obtained by numerical simulations for tape architectures representative of samples S2 and S4, for $I = 80$ A and $R_i = 0.2 \mu\Omega cm^2$. The current in each layer was calculated as the integral of the current density J in the cross-section of the layer. In all cases, the normal zone was initiated at $x = 0$. The data shown above were taken at (a) $t = 15$ ms and (b) $t = 30$ ms.

direction) for samples S2 and S4 obtained from numerical simulations. In both cases, the current is flowing in the superconductor until it reaches the normal zone, and then it transfers into the stabilizer (top and bottom layers) and into

the substrate. In the case of sample S2, we see from figure 5(a) that most of the current transfers from the superconductor to the bottom stabilizer layer, while in the case of sample S4 (figure 5(b)), most of the current transfers from the superconductor to the top stabilizer layer, which confirms the validity of the model based on two resistances in parallel. Furthermore, we note that, in the case of sample S2, the current transfers from the superconductor to the metallic layers over a length of approximately 10 mm. However, in the case of sample S4, we observe that it takes less than 1 mm for the current to transfer from the superconductor to the metallic layers (figure 5(b)). This clearly shows that the ‘b-CFD’ architecture increases the CTL, which is the key to increase the NZPV [17]. Indeed, the NZPV is proportional to the longest length between the thermal diffusion length and the CTL in the case of a uniform resistive layer [8]. The consequence of a longer CTL is that the heat is generated not only in a region close to the normal zone, but also away from it, i.e. the heat generation spreads over a much greater distance in front of the normal zone. After a local quench occurs, the current flows in the layer with the lowest resistance, which is located on the bottom of the tape in the case of the b-CFD architecture. To reach that layer, the current must transfer over a certain length, which corresponds to the CTL. This length is much longer compared to that of commercial tapes, where the majority of the current transfers to the stabilizer located on top of the tape.

The quenching behavior of the HTS tapes investigated in this work can thus be understood by comparing the paths taken by the current when transferring from the (RE)BaCuO layer to the Ag stabilizer for the two extreme cases, i.e. $t_{\text{top}} = 0.02 \mu\text{m}$ and $t_{\text{top}} = 2.0 \mu\text{m}$. In the case where all Ag is deposited on the (RE)BaCuO side ($t_{\text{top}} = 2 \mu\text{m}$), the current goes directly into the top Ag layer without seeing resistance, as it circumvents the quenched region. This architecture is typical of commercial tapes and possesses the lowest NZPV. When $t_{\text{top}} = 0.02 \mu\text{m}$, almost all the current is forced to transfer to the bottom stabilizer through the Ag bridges located on the edges of the tape, and therefore a significant electrical resistance is seen by the current (see [17] for more details). This higher resistance increases the CTL and thus, the NZPV [8].

7. Conclusion

In this paper, we introduced an original architecture for the metallic thermal stabilizer required in (RE)BaCuO high temperature superconductor (HTS) tapes. This new architecture was called ‘b-CFD’, standing for ‘buffer-CFD’, since it consists of an implementation of the CFD concept [6] by using the electrical insulation properties of the buffer layers, already present in existing HTS tapes. Similarly as in the original CFD concept, the b-CFD architecture allows increasing substantially the NZPV of the tapes by concentrating the generation of the Joule losses at specific locations in the tape when the current transfers between the superconducting and stabilizer layers to circumvent a hot spot. However, as opposed to the classical CFD concept, the

b-CFD architecture does not increase the interfacial resistance between the stabilizer and the superconductor. Furthermore, the b-CFD architecture allows for increasing the NZPV even in the presence of a thick stabilizer, which is not the case for the classical CFD architecture [17]. This is particularly interesting for applications requiring a thick stabilizer such as HTS superconducting magnets, for which efficient quench protection strategies have been sought for a long time. To diminish Joule losses during the current decay after a quench, numerical simulations predict that it is possible to retain the b-CFD effect while using a thick bottom stabilizer. From a practical point of view, a metal such as copper can be electrodeposited quickly and cheaply directly on the silver (bottom side) to reach a thickness in the range of 20–40 μm . Note that the development of HTS tapes for high-field magnets is expected to become one of the main drivers in this industry, so the b-CFD approach might be worth further investigations.

Now that the b-CFD architecture is well proven in terms of effectiveness and simplicity, the last challenge is to find a way to process it rapidly over long lengths of HTS tapes (hundreds of meters). One needs to find a good combination of low-cost metallization processes, such as electroless plating or electrodeposition. The process also needs to reliably ensure the electrical connection between the top and bottom stabilizers along the full tape length. Finally, the very low thickness (≈ 20 –100 nm) required for the top Ag stabilizer might be the major difficulty to overcome, since thin Ag layers may form aggregates under heat treatment, such as that used in the final oxygenation of the superconducting layer of HTS tapes.

Acknowledgments

The authors gratefully thank the support of Superconductor Technologies Inc. (STI). This work was supported by research grants from NSERC (Canada) and FRQNT (Québec).

ORCID iDs

J-H Fournier-Lupien  <https://orcid.org/0000-0002-0792-2548>

References

- [1] Senatore C, Alessandrini M, Lucarelli A, Tediosi R, Uglietti D and Iwasa Y 2014 *Supercond. Sci. Technol.* **27** 103001
- [2] Maeda H and Yanagisawa Y 2014 *IEEE Trans. Appl. Supercond.* **24** 4602412
- [3] Trociewitz U P, Dalban-Canassy M, Hannion M, Hilton D K, Jaroszynski J, Noyes P, Viouchkov Y, Weijers H W and Larbalestier D C 2011 *Appl. Phys. Lett.* **99** 202506
- [4] Bird M D, Dixon I R and Toth J 2015 *IEEE Trans. Appl. Supercond.* **25** 4300606
- [5] Lacroix C, Fournier-Lupien J H, Mcmeekin K and Sirois F 2013 *IEEE Trans. Appl. Supercond.* **23** 4701605

- [6] Lacroix C, Lapierre Y, Coulombe J and Sirois F 2014 *Supercond. Sci. Technol.* **27** 055013
- [7] Lacroix C and Sirois F 2014 *Supercond. Sci. Technol.* **27** 035003
- [8] Levin G A, Novak K A and Barnes P N 2010 *Supercond. Sci. Technol.* **23** 014021
- [9] Duckworth R C 2001 Contact resistance and normal zone formation in coated yttrium barium copper oxide superconductors *PhD Thesis* University of Wisconsin-Madison http://fs.magnet.fsu.edu/~lee/asc/pdf_papers/theses/rcd01phd.pdf
- [10] Grabovickic R, Lue J W, Gouge M J, Demko J A and Duckworth R C 2003 *IEEE Trans. Appl. Supercond.* **13** 1726–30
- [11] Wang X, Caruso A R, Breschi M, Zhang G, Trociewitz U P, Weijers H W and Schwartz J 2005 *IEEE Trans. Appl. Supercond.* **15** 2586–9
- [12] Armenio A A *et al* 2008 *IEEE Trans. Appl. Supercond.* **18** 1293–6
- [13] Wang X, Trociewitz U P and Schwartz J 2009 *Supercond. Sci. Technol.* **22** 085005
- [14] Park H Y, Kim A R, Park M, Yu I K, Eom B Y, Bae J H, Kim S H, Sim K and Sohn M H 2010 *IEEE Trans. Appl. Supercond.* **20** 2122–5
- [15] Lu W J, Fang J, Li D, Wu C Y and Guo L J 2013 *Physica C* **484** 153–8
- [16] Chan W K, Masson P J, Luongo C A and Schwartz J 2009 *IEEE Trans. Appl. Supercond.* **19** 2490–5
- [17] Lacroix C, Sirois F and Fournier Lupien J H 2017 *Supercond. Sci. Technol.* **30** 064004
- [18] Matias V, Rowley E J, Coulter Y, Maiorov B, Holesinger T, Yung C, Glyantsev V and Moeckly B 2009 *Supercond. Sci. Technol.* **23** 014018
- [19] Ekin J W 2006 *Experimental Techniques for Low-Temperature Measurements* (Oxford: Oxford University Press)
- [20] Kraemer H P, Schmidt W, Utz B and Neumueller H W 2003 *IEEE Trans. Appl. Supercond.* **13** 2044–7
- [21] Nam K, Kang H, Lee C, Ko T K and Seok B Y 2006 *IEEE Trans. Appl. Supercond.* **16** 727–30
- [22] Nguyen N T and Tixador P 2009 *Supercond. Sci. Technol.* **23** 025008
- [23] Nguyen N T, Barnier C and Tixador P 2010 *J. Phys.: Conf. Ser.* **234** 032058
- [24] Brandt E H 1996 *Phys. Rev. B* **54** 4246–64
- [25] Polat A, Sinclair J W, Zuev Y L, Thompson J R, Christen D K, Cook S W, Kumar D, Chen Y and Selvamanickam V 2011 *Phys. Rev. B* **84** 024519
- [26] Dresner L 2002 *Stability of Superconductors* (Dordrecht: Kluwer Academic)
- [27] Levin G A, Barnes P N and Bulmer J S 2007 *Supercond. Sci. Technol.* **20** 757–64